Journal of Statistical Physics, Vol. 81, Nos. 3/4, 1995

Stationary States of Crystal Growth in Three Dimensions

D. J. Gates[1] and M. Westcott[1]

Received November 1, 1994; final May 8, 1995

A new Markov process describing crystal growth in three dimensions is introduced. States of the process are configurations of the crystal surface, which has a terrace–edge–kink structure. The states are continuous along edges but discrete across edges, in accordance with the very different rates for the two types of captures of particles. Stationary distributions, describing steady crystal growth, are found in general. To our knowledge, these are the first examples of stationary distributions for layered crystal growth in three dimensions. The steady growth rate and other quantities are obtained explicitly for two interacting edges. For many interacting edges, growth behavior is determined (a) in various asymptotic regimes including thermodynamic limits, (b) via simulations, and (c) using series (cluster) expansions in the slope of the surface, the first three coefficients being computed. The theoretical growth rates show a marked dependence on surface dimensions. This may contribute to the size dependence and dispersion in the observed growth rate of small crystals.

KEY WORDS: Crystal growth; Markov process; stationary distribution; growth rate; thermodynamic limit; cluster expansion; coincidence probability; simulation; solid-on-solid.

1. INTRODUCTION

Crystal growth can be described by Markov processes whose states are configurations of the crystal edge (in two dimensions) or surface (in three dimensions) and whose transitions are captures and escapes of particles therefrom (e.g., refs. 14, 18, and 32). One can give a mathematically exact analysis of steady states of growth in two dimensions[12,13,10,16] and this has application to polymer crystallization,[7,21,22,25,27,30] where the crystals are flat or *lamellar*. The analysis in refs. 13, 10, and 16 provides explicit

[1] CSIRO Division of Mathematics and Statistics, G.P.O. Box 1965, Canberra ACT 2601, Australia.

0022-4715/95/1100-0681$07.50/0

stationary distributions, steady growth rates, and other quantities for a physically relevant class of transition rates. These transitions rates lead to a form of detailed balance and to the *dynamic reversibility* of the process. For more general transition rates, such distributions are unknown, but existence conditions have been found.[15]

Three-dimensional crystal growth has been studied intensively for a long time, in hundreds of publications, using computer simulation and various approximations (e.g., refs. 8, 18, 19, 32, 26, and 23), and much physical insight has been gained. Mathematical understanding of three-dimensional crystal growth is much more limited. Some existence conditions are known,[14,15] but there are no exact solutions for steady growth analogous to the two-dimensional ones. There is no discrete event Markov model where a stationary distribution, under net growth conditions, is known. Hence there is no partition function from which one might try to deduce macroscopic behavior. Further, one can prove[14] that a significant class of models has no dynamically reversible members. So stationary distributions might be quite complex and difficult to find. These basic deficiencies have been a major barrier to a deeper understanding of the physics of crystal growth.

2. THE NEW MODEL

To circumvent these difficulties, we consider a model that is discrete in one direction on the crystal surface, but continuous in the other. The crystal grows on a rectangular base (or substrate) of length L and integer breadth B (Figs. 1a and 1b). The breadth is divided into *terraces* or *levels* $l = 1, 2, \ldots, A$, where level $l+1$ is unit distance higher than level l. Periodic boundary conditions are used, so that level $A+1$ is identified with level 1.

The edge of level l, where it falls to level $l-1$, has N_l unit steps or *kinks* facing west at (real-valued) locations $x_{l1}, \ldots, x_{lN_l}$ and N_l unit kinks facing east at locations $y_{l1}, \ldots, y_{lN_l}$, as shown in Fig. 2. We call this edge number l. Edges 1, 2, ..., A are shown in Fig. 1b and the periodic image of edge A is shown as a broken line (see also Fig. 10). The configuration or state $\mathbf{C}$ of the process comprises these variables, subject to

$$\begin{aligned} 0 \leqslant x_{l1} \leqslant \cdots \leqslant x_{lN_l} < L \\ 0 \leqslant y_{l1} \leqslant \cdots \leqslant y_{lN_l} < L \end{aligned} \tag{2.1}$$

for each l, together with the NS locations $z_1, \ldots, z_A$ of the edges, measured southward from the NW corner on the western border of the substrate (Fig. 1b). These latter are integers subject to

$$1 \leqslant z_1 \leqslant \cdots \leqslant z_A \leqslant B \tag{2.2}$$

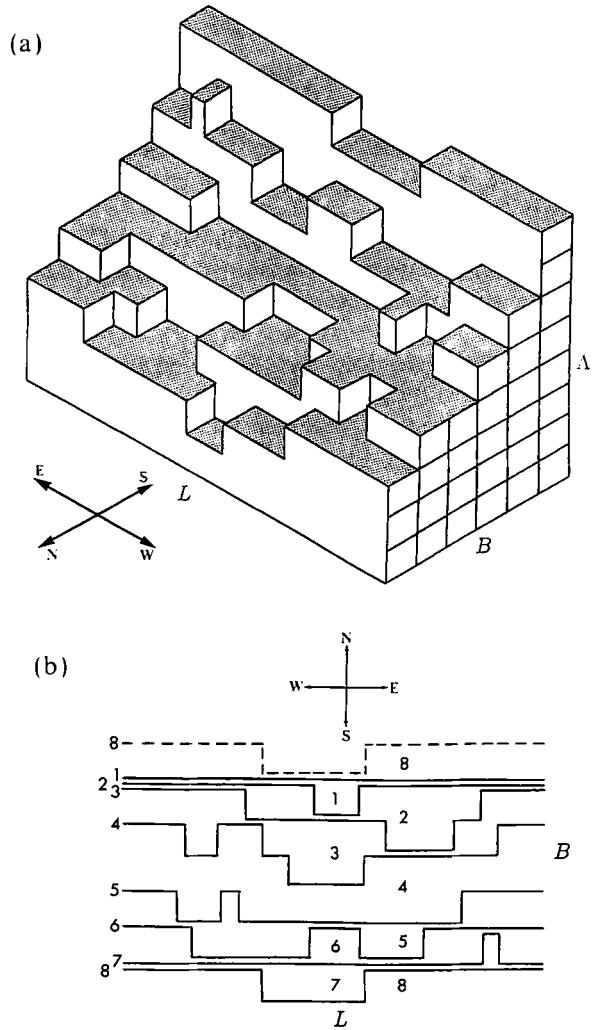

Fig. 1. The crystal surface, indicating the A terraces and their edges and kinks. (a) A perspective drawing with terraces shaded, (b) projection of (a) on the (B, L) plane.

Periodic boundary conditions in the L direction imply that a state with $x_{lr} = L$ and given z_l is identified with the state having $x_{lr} = 0$ and corresponding edge location $z_l + 1$. Similarly, $(y_{ls} = L; z_l)$ is indentified with $(y_{ls} = 0; z_l - 1)$.

The state space Ω comprises all such **C**'s where terraces have no overhangs; that is, the "solid-on-solid" (SOS) rule is obeyed. This means that edges, as viewed in Fig. 1b, do not overlap.

Fig. 2. Kink locations on edge number l.

We define a continuous-time Markov process on this state space as follows. Atoms are captured by the surface in two ways.[7] A type 1 capture is the attachment of a square *card* and is represented by a new *spike* on an edge, as shown in Fig. 3, leading to a new configuration with an added $x_{lr} = y_{ls}$. This is possible only when it does not violate the SOS rule. The captures comprise a Poisson process in time and are uniform on the allowed intervals of the edge, with rate i spikes per unit EW distance per unit time. Type 2 captures occur on the faces of kinks and result in the simultaneous EW motion of all kinks with speed g in the sense in which they face (Fig. 3). These evidently never violate the SOS rule. Neighboring kinks moving together and *recombining* constitutes a further transition, in which an $x_{lr} = y_{ls}$ is deleted from **C**. West-moving kinks that reach 0 reappear at L and east-moving kinks that reach L reappear at 0.

Our process is essentially a multiedge version of the model of ref. 1, with extra SOS rule exclusions. The continuous nature of the process in the EW direction implies that type 2 captures are very frequent compared to type 1's. Predominance of type 2's is typical when crystal growth is not too fast; type 2 sites are more attractive because there are more neighbor atoms to bond to. If the edges are rather smooth, coincident like-kinks will not occur, so the edges will have the structure described. This can be made precise as shown in refs. 12, 13, and 16. Thus the model is physically natural in spite of its asymmetry. The other conceivable captures—atoms on a flat surface—are excluded. For real crystals, these *nucleations* are infrequent compared to the other captures unless growth rate or temperature is high,[6,32] in which case a different model would be needed.

For macroscopic theory, A and B will be large. Then the periodicity will not be felt, and the model will represent a surface with slope A/B in

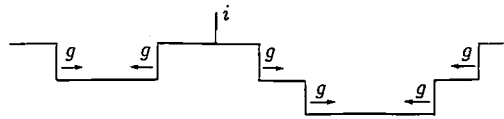

Fig. 3. Captures of type 1 (spike) and type 2 (speed g).

the NS direction. Alternatively, the edges can be regarded as originating from screw dislocations.[6,32]

Although the state space treats A and B differently, it is clear from Fig. 1a that the process is the same if A and B are interchanged. This fact will be exploited to relate results at low and high values of A/B.

The model can be generalized to include a slope in the EW direction; for example, give every edge an excess of K left-facing kinks.[16] To avoid excessive complexity, we postpone this generalization until Section 15.

The physical process of melting or evaporation of a crystal surface by escape of atoms can be treated by using what is essentially a reversed version of the present process. (See ref. 10, Section 5. This reference gives a mathematical version of the Wilson–Frenkel theory.)

3. THE FORWARD EQUATION

The probability density at time t of state $\mathbf{C}$ having total number

$$N = \sum_{l=1}^{\Lambda} N_l \tag{3.1}$$

of left kinks is denoted $P_N(\mathbf{C}, t)$. To write the forward equation we consider three cases.

Case 1. $x_{lr} \neq y_{ls}$, $x_{lr} \neq 0$, L, and $y_{ls} \neq 0$, L for all l, r, s. Then the following transitions contribute. A spike could be created on edge l (on level $l-1$) at any point u in a set $S_l(\mathbf{C}) \subset L$ where there is space between edges $l-1$ and l (Fig. 4). Or a recombination of two kinks could have occurred anywhere in S_{l+1}. We write $H_l(u, \mathbf{C})$ for the indicator function of S_l (i.e., 1 for u in S_l and 0 otherwise) and $D_l(\mathbf{C})$ for its total length. Then the forward equation is

$$\begin{aligned}\frac{\partial}{\partial t} P_N(\mathbf{C}, t) = &-iP_N(\mathbf{C}, t) \sum_{l=1}^{\Lambda} D_l(\mathbf{C}) \\ &+ 2g \sum_{l=1}^{\Lambda} \int_0^L du\, P_{N+1}[\{\mathbf{C}, (u, u)_l\}, t]\, H_{l+1}(u, \mathbf{C}) \\ &+ g \sum_{l=1}^{\Lambda} \sum_{r=1}^{N_l} \left(\frac{\partial}{\partial x_{lr}} - \frac{\partial}{\partial y_{lr}} \right) P_N(\mathbf{C}, t)\end{aligned} \tag{3.2}$$

where $\{\mathbf{C}, (u, u)_l\}$ means that u is appended to the x_l's and to the y_l's. The first term describes type 1 captures, producing transitions out of $\mathbf{C}$. The second term describes recombinations of kinks which lead into state $\mathbf{C}$. The final term describes the deterministic motion of kinks with speed g.

For the case of one layer ($\Lambda = 1$) (3.2) is essentially the equation of Bennett *et al.*[1] They include coincidences of kinks by means of Dirac delta functions. We consider these separately.

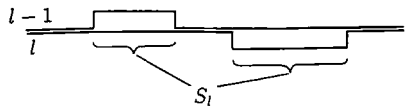

Fig. 4. Example of a set S_l where spikes can occur on edge l and kinks could have recombined on edge $l-1$.

Case 2. $x_{lr} = y_{ls} = u$, say, while $x_{mu} \neq 0, L$ and $y_{mv} \neq 0, L$ for all m, u, v. Then the forward equation is

$$\frac{\partial}{\partial t} P_N(\mathbf{C}, t) = \text{RHS of (3.2)} + i \sum_{l=1}^{\Lambda} P_{N-1}(\mathbf{C}_{lrs}, t)\, H_l(u, \mathbf{C}) - 2gP_N(\mathbf{C}, t) \sum_{l=1}^{\Lambda} H_{l+1}(u, \mathbf{C}) \tag{3.3}$$

where $\mathbf{C}_{lrs}$ is the result of removing x_{lr} and y_{ls} from $\mathbf{C}$. We have omitted the obvious Dirac delta functions.

Overflow Cases. If a kink crosses 0 or L, there is relabelling of the x's or y's and a jump in a z coordinate. Thus, for our choice of state variables, there is a jump transition, though this is not a physical transition. First consider a state $\mathbf{C}$ with $x_{l1} < y_{l1}$ and $0 < x_{l1} < g\,dt$ at time t. For small enough dt, this will hold for at most one l. It follows that (within order dt) $z_l \geqslant z_{l-1} + 1$ and there will be no creations or recombinations or overflows at L during $(t, t+dt)$ [since such simultaneous events have probability of order $(dt)^2$]. Then the kink at x_{l1} will reach $x_{l1} - g\,dt + L$ at time $t+dt$. First exclude the case where both $l=1$ and $z_1 = 1$. Then the state $\mathbf{C}'$ at $t+dt$ is given by

$$\begin{aligned} x'_{lN_l} &= x_{l1} - g\,dt + L \\ x'_{lr} &= x_{l,r+1} - g\,dt \qquad \text{for} \quad r = 1,\ldots, N_l - 1 \\ x'_{mr} &= x_{mr} - g\,dt \qquad \text{for} \quad m \neq l, \quad \text{all } r \\ y'_{mr} &= y_{mr} + g\,dt \qquad \text{for all } m, r \\ z'_l &= z_l - 1 \\ z'_m &= z_m \qquad \text{for all} \quad m \neq l \end{aligned} \tag{3.4}$$

If, however, $l=1$ and $z_1 = 1$, then the new z's are

$$\begin{aligned} z'_l &= z_{l+1} \qquad \text{for} \quad l = 1,\ldots, \Lambda - 1 \\ z'_\Lambda &= B \end{aligned} \tag{3.5}$$

Then

$$P_N(\mathbf{C}', t+dt) = P_N(\mathbf{C}, t) + o(1) \tag{3.6}$$

A similar equation holds if $x_{lN_l} < y_{lN_l}$ and $L - g\,dt < y_{lN_l} < L$ at time t.

Since simultaneous type 1 captures are zero measure events, we need not consider them; likewise for simultaneous recombinations and simultaneous overflows of kinks at the ends of $[0, L)$. Thus (3.2), (3.3), and (3.6) suffice to describe the time development of P_N for initial states of physical interest.

4. THE STATIONARY DISTRIBUTION AND DYNAMIC REVERSIBILITY

We show that the stationary distribution is

$$\Pi_N(\mathbf{C}) = (i/2g)^N/Z, \qquad \mathbf{C} \in \Omega \tag{4.1}$$

where Z is the normalizing constant or partition function. Thus $\Pi_N(\mathbf{C})$ is uniform on each subset of Ω having fixed N. To prove that $\Pi_N(\mathbf{C})$ is normalizable, we write

$$Z = \sum_{\mathbf{N}} \eta^{2N} V_{\mathbf{N}} \tag{4.2}$$

where $\eta = (i/2g)^{1/2}$, $\mathbf{N} = (N_1, \ldots, N_\Lambda)$ and $V_{\mathbf{N}}$ is the volume of the subset $\Omega_{\mathbf{N}}$ of the state space Ω with kinks $\mathbf{N}$, and involves integrals with respect to the x_{l_r}'s and y_{l_r}'s and sums over the z_l's. Relaxing the SOS rule gives the bound

$$V_{\mathbf{N}} \leqslant \binom{B+\Lambda-1}{\Lambda} \prod_{l=1}^{\Lambda} \left(\frac{L^{N_l}}{N_l!}\right)^2 \tag{4.3}$$

where the combinatorial factor V_0 is the number of distinct combinations of z_l's. Thus the sum (4.2) converges and has the bound

$$Z \leqslant V_0 I_0^\Lambda(2\eta L) \tag{4.4}$$

where $I_0(\cdot)$ is the modified Bessel function.

To establish (4.1), we note that it reduces the right side of (3.2) to

$$-i\Pi_N \sum_l D_l + 2g\Pi_{N+1} \sum_l D_{l+1} \tag{4.5}$$

Since the D_l's are periodic ($D_{\Lambda+1} = D_1$), (4.5) is zero. The right side of (3.3) reduces to

$$i\Pi_{N-1} \sum_l H_l - 2g\Pi_N \sum_l H_{l+1} \tag{4.6}$$

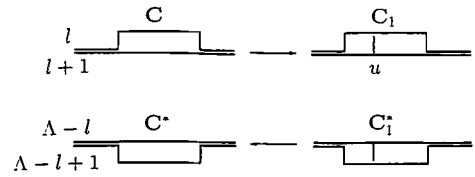

Fig. 5. A type 1 transition and the reverse transition through the conjugate states.

Since the H_l's are also periodic, (4.6) is zero, too. Further, (3.6) is satisfied by Π_N because of the above uniformity of Π_N. Thus (4.1) is established, though certain questions of mathematical rigor (definition, existence, and uniqueness) have not been considered.

We note that (4.1) reduces to the Bennett *et al.* result[1] when $\Lambda = 1$. Their derivation is much more complex, though basically equivalent for $\Lambda = 1$. They give a heuristic argument as well.

One can get some mathematical insight into the process and the simplicity of its stationary distribution as follows. For any $\mathbf{C}$ define the conjugate state $\mathbf{C}^*$ as the result of reflecting the picture in Fig. 1b so that north and south are interchanged. Equivalently, interchange the x_{lr}'s and y_{ls}'s for each l, and reverse the order of the edges thus

$$z_l^* = B + 1 - z_{\Lambda+1-l}$$
$$x_{lr}^* = y_{\Lambda+1-l,r}$$
$$y_{lr}^* = x_{\Lambda+1-l,r}$$

Evidently $(\mathbf{C}^*)^* = \mathbf{C}$ and we note that $S_l(\mathbf{C}) = S_{\Lambda+2-l}(\mathbf{C}^*)$. It is clear from (4.1) that (omitting N from the notation)

$$\Pi(\mathbf{C}^*) = \Pi(\mathbf{C}) \tag{4.7}$$

Now we write $\mathbf{C}_1$ for the state $\{\mathbf{C}, (u, u)_{l+1}\}$ and $q(\mathbf{C}, \mathbf{C}')$ for the (possibly zero) transition rate from state $\mathbf{C}$ to any state $\mathbf{C}'$. Thus

$$q(\mathbf{C}, \mathbf{C}_1) = iH_{l+1}(u, \mathbf{C}) \tag{4.8}$$

which describes the creation of a spike at u on edge $l+1$ (Fig. 5). The transition $\mathbf{C}_1^* \to \mathbf{C}^*$ is a recombination of kinks (Fig. 5) and has rate

$$q(\mathbf{C}_1^*, \mathbf{C}^*) = 2gH_{\Lambda+1-l}(u, \mathbf{C}^*) = 2gH_{l+1}(u, \mathbf{C}) \tag{4.9}$$

Since $\Pi(\mathbf{C})i = \Pi(\mathbf{C}_1)\,2g$, we conclude that

$$\Pi(\mathbf{C})\, q(\mathbf{C}, \mathbf{C}_1) = \Pi(\mathbf{C}_1^*)\, q(\mathbf{C}_1^*, \mathbf{C}^*) \tag{4.10}$$

Writing $\mathbf{A}_1 = \mathbf{C}_1^*$ and $\mathbf{A} = \mathbf{C}^*$, (4.10) becomes

$$\Pi(\mathbf{A}_1)\, q(\mathbf{A}_1, \mathbf{A}) = \Pi(\mathbf{A}^*)\, q(\mathbf{A}^*, \mathbf{A}_1^*) \tag{4.11}$$

where $\mathbf{A}_1 \to \mathbf{A}$ is a recombination transition. Equations (4.10) and (4.11) show that a form of detailed balance holds for all transitions. The total rate of all transitions out of $\mathbf{C}$ is

$$q(\mathbf{C}) = i \sum_l D_l \tag{4.12}$$

if no x_{lr} coincides with a y_{ls}. If $x_{lr} = y_{ls} = u$, then

$$q(\mathbf{C}) = i \sum_l D_l + 2g \sum_l H_{l+1}(u, \mathbf{C}) \tag{4.13}$$

It follows easily that

$$q(\mathbf{C}^*) = q(\mathbf{C}) \tag{4.14}$$

for all $\mathbf{C}$. Equations (4.7), (4.10), (4.11), and (4.14) are the basic balance equations that characterize a *dynamically reversible* process,[33,34] i.e., the stationary process $\mathbf{C}^*(t)$ is identical to the stationary process $\mathbf{C}(\tau - t)$ for any τ. This is not established rigorously, because we have not set up the appropriate probabilistic formalism, but it is fairly evidently true (it was this observation that led us to the model in the first place).

Most multidimensional Markov processes, with known stationary distributions, satisfy some form of reversibility and associated balance conditions. Conversely, many studies have been limited by the absence of such a property and the consequent absence of a known stationary distribution. We have shown that a significant class of fully discrete, crystal growth models, in three dimensions, do not have such a property[14]; there is a function $\Pi(\mathbf{C})$ which satisfies equations of the form (4.10), but (4.14) does not hold for all $\mathbf{C}$ (as in ref. 8, for example). Thus there is a fundamental obstacle to progress with such models.

5. STATISTICAL QUANTITIES AND GROWTH REGIMES FOR SMALL AND LARGE CRYSTALS

The growth rate, or captured area in unit time, per unit substrate area is

$$G = \frac{2g}{LB} \left\langle \sum_l N_l \right\rangle = \frac{g\eta}{L} \frac{\partial \phi}{\partial \eta} \tag{5.1}$$

where $\langle \cdot \rangle$ denotes expectation with respect to Π over all N and

$$\phi = \frac{1}{B} \log Z \tag{5.2}$$

By analogy with equilibrium statistical mechanics, we refer to $-\phi$ as the *free energy*. The growth speed in the direction normal to the crystal surface is $(1 + A^2/B^2)^{-1/2} G$. The creation rate per unit substrate area is iR, where

$$R = \frac{1}{LB} \left\langle \sum_l D_l \right\rangle \tag{5.3}$$

which is an indicator of the degree of interaction between edges. Correlations among the N_l and the D_l are also of interest.

Let σ denote the proportion of the A adjacent edge pairs that touch. Then $1 - \langle \sigma \rangle$ is the probability that edges 1 and 2 (say) do not touch. The resulting gap of one site in the NS direction implies that

$$1 - \langle \sigma \rangle = Z(A, B-1)/Z(A, B) \tag{5.4}$$

The quantity

$$\bar{p}(A, B) \equiv -\log[1 - \langle \sigma \rangle] \tag{5.5}$$

which we call the *pressure*, is a measure of the "horizontal" crowding of edges. Evidently $\bar{p}(A, 1) = \infty$.

Let $P(a_1, ..., a_n, b_1, ..., b_n | n)$ denote the probability that $z_1 = z_2$ and $|x_{1r} - x_{2r}| < a_r$ and $|y_{1r} - y_{2r}| < b_r$ for every r, conditional on there being n x-kinks on each of edges 1 and 2. Then, as every $a_r, b_r \to 0$,

$$\left\langle P(a_1, ..., b_n \mid n) \Big/ \prod_{r=1}^{n} a_r b_r \right\rangle \to Z(A-1, B)/Z(A, B) \equiv \bar{\zeta}(A, B), \qquad \text{say} \tag{5.6}$$

which we call the *activity*. It gives the concentration of probability density at the coincidence of two edges, and is a measure of the "vertical" crowding of edges.

Obviously, $\bar{p}$ and $\bar{\zeta}$ are mathematical analogs of their namesakes in the equilibrium statistical mechanics of fluids, though their physical interpretations are different.

Since A and B are interchangeable, $\mathcal{N}(A, B) = \mathcal{N}(B, A)$, where $\mathcal{N} = \langle \sum_l N_l \rangle$, and so

$$G(A, B) = (A/B)\, G(B, A) \tag{5.7}$$

The probability that there are no kinks on any edge is V_0/Z. Equating this to its value when A and B are interchanged gives

$$AZ(A, B) = BZ(B, A) \tag{5.8}$$

which implies that

$$\phi(A, B) = (B/A)\,\phi(B, A) + (1/B)\log(B/A) \tag{5.9}$$

and

$$\bar{p}(A, B) = -\log \bar{\zeta}(B, A) + \log[B/(B-1)] \tag{5.10}$$

These have special relevance in the thermodynamic limit [see (10.31)].

An easy calculation [see (4.4)] gives $Z(1, B) = BI_0(2\eta L)$ and

$$G(1, B) = \frac{(2ig)^{1/2} I_1(2\eta L)}{BI_0(2\eta L)} = \frac{1}{B} G(B, 1) \tag{5.11}$$

References 1, 13, and 20 give $G(1, 1)$. In Section 6 we analyze a two-edge model. For many edge models, we obtain cluster expansions (Section 13), perform simulations (Section 14), and consider various asymptotic regimes:

Regime I: few kinks (small ηL), Section 7

Regime II: many kinks (large ηL), Section 8

Vicinal surfaces: small and large A/B, Section 9

Thermodynamic limit, grand ensemble: A, $B \to \infty$, $A/B \to \rho$, Sections 10–12.

The continuous EW state variables imply that, for any finite L, the EW length is very large on an atomic or molecular scale, and L is a rescaled length. For a single edge, a discrete model with M EW sites (atoms) can be analyzed[13,16] and our continuous model obtained with the identification

$$M\alpha \to Li, \qquad \nu/M \to g/L \tag{5.12}$$

as $\alpha \to 0$ and M, $\nu \to \infty$, where α and ν are rates of the discrete model. Thus, the further limit $L \to \infty$ in regime II has an essentially different interpretation from $B \to \infty$.

For fixed η, regimes I and II (names borrowed from polymer crystallization[7,16]) correspond, on the whole, to small and large crystals. Small crystals are important in many industrial processes involving separation and purification from solutions.[9] The rates of such processes are

dominated by the growth rates of small crystals. The growth rates often show a marked size dependence (e.g., Fig. 9 in ref. 9) as well as a variation among crystals of the same size—so-called growth rate dispersion. The distinctly different growth rates through regimes I to II [see Fig. 6a and Eq. (8.3)] may contribute to this phenomenon. Other explanations involving dislocations and surface-to-volume ratio (ref. 9, Section 4.3) have been offered, but the question is not fully resolved. Because of these considerations, we shall seek results applicable for all L.

6. THE TWO-EDGE MODEL

For the case $\Lambda = 2$, the partition function can be evaluated explicitly as follows. Setting $d = z_2 - z_1$ and using the NS periodicity, we have

$$Z(2, B) = \frac{1}{2} B \sum_{d=0}^{B} \sum_{N_1=0}^{\infty} \sum_{N_2=0}^{\infty} \frac{(\eta L)^{2(N_1+N_2)}}{[2(N_1+N_2)]!} \#(2N_1, 2N_2, d; B) \quad (6.1)$$

where $\#(\cdot)$ is the number of arrangements of $2N_l$ kinks on edge l (N_l of each type, $l = 1, 2$) which ensure they never cross if they start d apart. Now assign the value $+1$ to the N_1 x-kinks on edge 1 and to the N_2 y-kinks on edge 2, all other kinks getting the value -1. Let the $+1$'s and -1's be the steps in a one-dimensional walk which begins at d [and ends at d after $2(N_1+N_2)$ steps]. Then, clearly, the walk stays within $[0, B]$ if and only if the original edges never cross. Evidently, the counting of walks requires only knowledge of the sequence of ± 1's, not where they originally came from. So any of the $\binom{N_1+N_2}{N_1}$ arrangements of the x-kinks and y-kinks among the $+1$ steps gives the same walk. The same applies to the -1 steps. Thus any such walk derives from $\binom{N_1+N_2}{N_1}^2$ possible edge arrangements, and so

$$\#(2N_1, 2N_2, d; B) = \binom{N_1+N_2}{N_1}^2 v(N_1+N_2, d; B) \quad (6.2)$$

where $v(s, d; B)$ is the number of walks with steps ± 1 between $(0, d)$ and $(2s, d)$ that stay inside $[0, B]$. Thus

$$\begin{aligned} Z(2, B) &= \frac{B}{2} \sum_{d=0}^{B} \sum_{s=0}^{\infty} \sum_{j=0}^{s} \frac{(\eta L)^{2s}}{(2s)!} \binom{s}{j}^2 v(s, d; B) \\ &= \frac{B}{2} \sum_{d=0}^{B} \sum_{s=0}^{\infty} \frac{(\eta L)^{2s}}{(s!)^2} v(s, d; B) \end{aligned} \quad (6.3)$$

A standard result is (ref. 4, Chapter 3, Q.3)

$$v(s, d; B) = \sum_{k=-\infty}^{\infty} \left\{ \binom{2s}{s+k(B+2)} - \binom{2s}{s+k(B+2)+d+1} \right\} \tag{6.4}$$

where, in fact, the sum is finite. Now consider

$$\begin{aligned} I_n^2(2x) &= \sum_{i=0}^{\infty} \sum_{j=0}^{\infty} \frac{x^{2(i+j)+2n}}{i!\, j!(i+n)!\,(j+n)!} \\ &= \sum_{s=0}^{\infty} \frac{x^{2s+2n}}{s!(s+2n)!} \sum_{k=0}^{s} \binom{s}{k}\binom{s+2n}{k+n} \\ &= \sum_{s=0}^{\infty} \frac{x^{2s+2n}}{s!(s+2n)!} \binom{2s+2n}{s+n} \qquad [\text{ref. 28, p. 617, 4.2.5, 24}] \\ &= \sum_{t=n}^{\infty} \frac{x^{2t}}{(t!)^2} \binom{2t}{t+n} \end{aligned} \tag{6.5}$$

Leaving the k sum from (6.4) till last, we have

$$\begin{aligned} Z(2, B) = \frac{B}{2} \sum_{k=-\infty}^{\infty} & \left\{ (B+1) \sum_{s=|k|(B+2)}^{\infty} \frac{(\eta L)^{2s}}{(s!)^2} \binom{2s}{s+|k|\,(B+2)} \right. \\ & \left. - \sum_{d=0}^{B} \sum_{s=|k(B+2)+d+1|}^{\infty} \frac{(\eta L)^{2s}}{(s!)^2} \binom{2s}{s+|k(B+2)+d+1|} \right\} \\ = & \frac{1}{2} B(B+1) \sum_{k=-\infty}^{\infty} I^2_{|k|(B+2)}(2\eta L) \\ & - \frac{1}{2} B \sum_{d=0}^{B} \sum_{k=-\infty}^{\infty} I^2_{|k(B+2)+d+1|}(2\eta L) \end{aligned} \tag{6.6}$$

The second term is just

$$\frac{1}{2} B \left\{ \sum_{k=-\infty}^{\infty} I^2_{|k|}(2\eta L) - \sum_{k=-\infty}^{\infty} I^2_{|k|(B+2)}(2\eta L) \right\} \tag{6.7}$$

Using Neumann's identity

$$\sum_{k=-\infty}^{\infty} I^2_{|k|}(2\eta L) = I_0(4\eta L) \tag{6.8}$$

we have

$$Z(2, B) = \tfrac{1}{2}B(B+2) \sum_{k=-\infty}^{\infty} I^2_{|k|(B+2)}(2\eta L) - \tfrac{1}{2}BI_0(4\eta L) \tag{6.9}$$

This can be written as a finite sum using the identity [ref. 28, p. 697, special case of 7 (which contains some misprints)]

$$\sum_{k=-\infty}^{\infty} I^2_{k\nu}(z) = \frac{1}{\nu} \sum_{k=k_-}^{k_+} \alpha_k I_0\{2z \cos(k\pi/\nu)\} \tag{6.10}$$

where $k_\pm = \pm[\nu/2]$ and $[\cdot]$ denotes integer part, and

$$\alpha_k = 1 \qquad \text{for} \quad k \neq k_\pm$$

$$\alpha_{k_\pm} = \begin{cases} 1/2 & \text{for } \nu \text{ even} \\ 1 & \text{for } \nu \text{ odd} \end{cases}$$

Then (6.9) reduces to

$$Z(2, B) = \frac{1}{2} B \sum_k \alpha_k I_0\left(4\eta L \cos \frac{k\pi}{B+2}\right) \tag{6.11}$$

where the sum extends from $-[(B+2)/2]$ to $[(B+2)/2]$ excluding $k=0$. More explicitly, for integer $\beta \geqslant 1$,

$$\begin{aligned} Z(2, 2\beta) &= \beta + 2\beta \sum_{k=1}^{\beta} I_0\left(4\eta L \cos \frac{k\pi}{2\beta+2}\right) \\ Z(2, 2\beta-1) &= (2\beta-1) \sum_{k=1}^{\beta} I_0\left(4\eta L \cos \frac{k\pi}{2\beta+1}\right) \end{aligned} \tag{6.12}$$

For example $Z(2, 1) = I_0(2\eta L)$, which is a special case of (5.8) with (5.11). Further,

$$Z(2, 2) = 1 + 2I_0(2\sqrt{2}\,\eta L) \tag{6.13}$$

whence

$$G(2, 2) = \sqrt{2}(2ig)^{1/2} I_1(2\sqrt{2}\,\eta L)/[1 + 2I_0(2\sqrt{2}\,\eta L)] \tag{6.14}$$

which is plotted in Fig. 6a. Thus $G(2, 2) \sim (1/\sqrt{2})(2ig)^{1/2}$ as $\eta L \to \infty$, which is less than the independent-edges result $(2ig)^{1/2}$, a consequence of the interaction between edges.

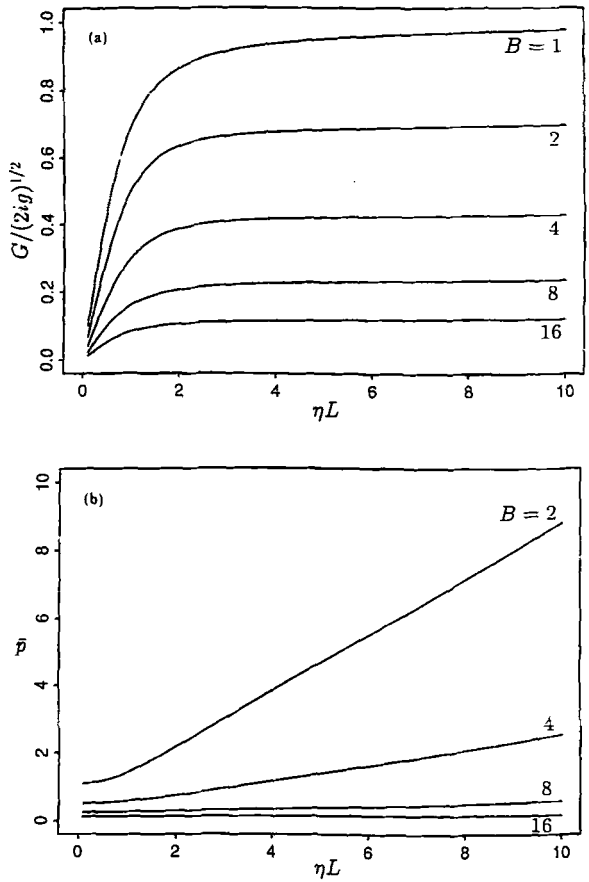

Fig. 6. Some results for the two-edge model. (a) Normalized growth rate versus ηL, (b) pressure versus ηL.

For large B, (6.9) gives $\bar{p} \sim \rho$ and

$$G \sim \rho G(1, 1) \tag{6.15}$$

where $\rho = 2/B$ is the edge density. These show, as expected, that the edges become noninteracting at low density. They are related to Theorem 2 of Section 9 and the cluster expansions (13.4) and (13.5).

For small ηL, implying low kink density, (6.12) gives

$$G(2, B) \sim 2Li/(B+1) \tag{6.16}$$

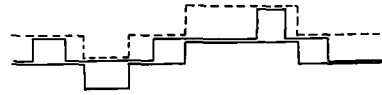

Fig. 7. An example with $B=1$.

which is a special case of Theorem 1 in Section 7. Similarly

$$\bar{p}(2, B) \sim \log \frac{B+1}{B-1} \tag{6.17}$$

For large ηL, (6.12) gives

$$G \sim (2ig)^{1/2} \frac{2}{B} \cos \frac{\pi}{B+2} \tag{6.18}$$

For $B=1$ (Fig. 7) this coincides with the general result (8.2), which implies $G(\Lambda, 1) \sim (2ig)^{1/2}$ as $\eta L \to \infty$. For large B, it coincides with the cluster expansion (13.5) to first order in ρ. Similarly, for $B>1$,

$$\bar{p}(2, B) \sim 4\eta L \left(\cos \frac{\pi}{B+2} - \cos \frac{\pi}{B+1} \right) \tag{6.19}$$

showing that the pressure is ultimately linear in ηL.

Figures 6a and 6b show G and $\bar{p}$ plotted against ηL for various ρ, using (6.12). These illustrate the relations (6.15)–(6.19). Figure 6a implies a dependence of growth rate on crystal size, and is in qualitative agreement with data such as Fig. 9 of ref. 9.

We note from (5.7) that $G(\Lambda, 2) = (\Lambda/2)\, G(2, \Lambda)$, which can be evaluated using (6.12).

7. REGIME I: SMALL ηL

Now we consider the many-edge model, beginning with small crystals. If $\eta L \ll 1$, then $iL \ll 2g/L$, so the time between creations on an edge is much greater than the time for a creation to grow and cover the edge. Then most edges are straight most of the time and form a set of straight steps. Each step may have height $\geqslant 1$ and their total height is Λ. The expected number of steps in such (equally probable) configurations is $B\Lambda/(\Lambda + B - 1)$. Since a creation covers an edge almost instantly, it contributes area iL per unit length per unit time. Thus one expects

$$G \sim L\Lambda i/(\Lambda + B - 1) \equiv G_0, \qquad \text{say} \tag{7.1}$$

in this regime. More precisely, we have the following result.

Theorem 1.

$$G/G_0 \to 1 \qquad \text{as} \quad \eta L \to 0 \tag{7.2}$$

for fixed A and B.

Proof. From (5.1), $G = 2gS/(LBZ)$, where

$$S = \sum_{N=1}^{\infty} N\mu(\Omega_N) \tag{7.3}$$

and

$$\mu(A) = \sum_{z} \sum_{N} \eta^{2N} \int d\{x\}_N \int d\{y\}_N I(A) \tag{7.4}$$

where $I(A)$ is the indicator of any set $A \subset \Omega$ and the sums and integrals extend over Ω. We bound S above and below as follows. First

$$S \geqslant \mu(\Omega_1) = B\mu(\Omega_{1,1}) \tag{7.5}$$

where $\Omega_{1,1} \subset \Omega_1$ is the state subspace where the edge carrying the kink pair has end point $z = 1$. In $\Omega_{1,1}$ the remaining $A - 1$ edges are straight and have $\binom{B+A-2}{A-1}$ distinct combinations of possible locations. If there is no other edge at 1, the kink pair can be in either order, and so the x and y integrations contribute L^2 to $\mu(\Omega_{1,1})$. If there is more than one edge at 1, then either the lowest edge can have kinks at $x < y$ (contributing $\frac{1}{2}L^2$) or the highest edge can have kinks at $x > y$ (again contributing $\frac{1}{2}L^2$), with total contribution L^2 again. Thus

$$\mu(\Omega_1) = B\binom{B+A-2}{A-1}\eta^2 L^2 \tag{7.6}$$

Using (4.4), we deduce that

$$G/G_0 \geqslant I_0^{-A}(2\eta L) \to 1 \qquad \text{as} \quad \eta L \to 0 \tag{7.7}$$

Next, $\mu(A) \leqslant \mu^*(A)$ for any $A \subset \Omega$, where the SOS rule is relaxed in μ^*. Thus

$$S \leqslant \mu(\Omega_1) + \sum_{N=2}^{\infty} N\mu^*(\Omega_N) \tag{7.8}$$

Since μ^* involves independent edges, we have

$$\mu^*(\Omega_N) = V_0 \sum_{\mathbf{N}} \prod_{l} \frac{(\eta L)^{2N_l}}{(N_l!)^2} \tag{7.9}$$

which yields

$$\sum_{N=2}^{\infty} N\mu^*(\Omega_N) = V_0 \Lambda (\eta L)^2 J \tag{7.10}$$

where

$$J = (\eta L)^{-1} I_1(2\eta L)\, I_0^{\Lambda - 1}(2\eta L) - 1 \tag{7.11}$$

Since $Z \geqslant V_0$ we have

$$G \leqslant G_0 + 2g\eta^2 L \Lambda J / B \tag{7.12}$$

whence

$$G/G_0 \leqslant 1 + J(B + \Lambda - 1)/B \tag{7.13}$$

But $I_1(2\eta L)/\eta L \to 1$ as $\eta L \to 0$, so that $J \to 0$. Theorem 1 then follows.

When there is an EW slope on the surface, the result is very different (Section 15).

8. REGIME II: LARGE ηL

In different contexts, de Gennes[17] and Villain and Bak[31] consider partition functions very similar to ours, and coinciding with ours in the limit $L \to \infty$. Their method involves expressing the partition function in terms of a transfer matrix which is the exponential of a free fermion Hamiltonian. The result [see (2.22) of ref. 31) in our notation is

$$\frac{\log Z(\Lambda, B)}{BL} \sim 2\eta \left(\frac{1+\rho}{\pi}\right) \sin\left(\frac{\rho\pi}{1+\rho}\right) \tag{8.1}$$

as $L \to \infty$, then Λ, $B \to \infty$, $\Lambda/B \to \rho$. The corresponding limiting growth rate is

$$G_\infty(\rho) = (2ig)^{1/2} \left(\frac{1+\rho}{\pi}\right) \sin\left(\frac{\rho\pi}{1+\rho}\right) \tag{8.2}$$

which satisfies the symmetry relation (10.31). In Fig. 8, $G_\infty(\rho)$ is plotted, together with simulations for $\eta L = 5$. The disparity for large ρ is due to the differing values of ηL: here kinks (creations) are discouraged by the crowding of edges, so the effect of finite ηL is more pronounced, and (8.2) is less relevant. The series expansion of $G_\infty(\rho)$ has no ρ^2 term; this has been given a physical explanation [e.g., ref. 2, Eq. (7.39)], but it is not true for finite L (Section 13).

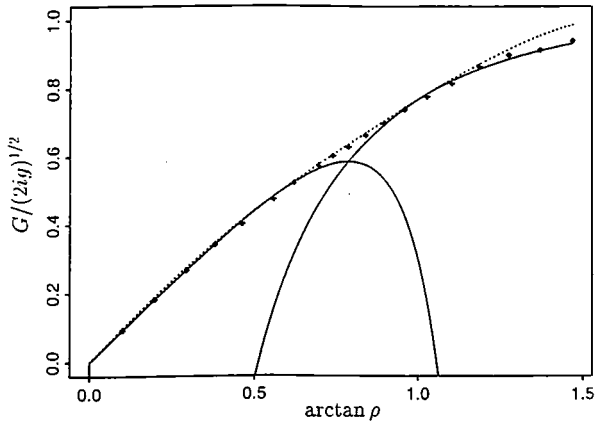

Fig. 8. Normalized growth rate versus angle of the surface in the model with $i = L = 1$, $g = 0.02$, and $\Lambda = 10$. The points are simulations, the solid lines are the cluster expansions (13.12) and (13.16), and the broken line is the regime II result (8.2).

Together with (7.1) we now have, for small ρ,

$$G \sim \begin{cases} \rho(2ig)^{1/2}(\eta L) & \text{if } \eta L \ll 1 \\ \rho(2ig)^{1/2} & \text{if } \eta L \gg 1 \end{cases} \tag{8.3}$$

which emphasizes the size dependence of growth rate (cf. ref. 9, Fig. 9). The surface of a small crystal may contain a population of edges with different lengths. Growth rate dispersion would then occur if this population varied among crystals.

Equation (6.18) can be derived also via the free fermion method[31] and for further results see ref. 23.

For polymer (two-dimensional) crystals, the explanation (8.3) for the observed size dependence of growth rate is well established.[7]

9. EXTREMES OF EDGE DENSITY: VICINAL SURFACES

If the density Λ/B of edges (surface slope) is low, one would expect the interaction between edges to be small. For regimes I and II this is established by (8.3). More generally we expect that $Z(\Lambda, B) \simeq Z^*(\Lambda, B)$, where

$$Z^*(\Lambda, B) = V_0 I_0^{\Lambda}(2\eta L) \tag{9.1}$$

which ignores the SOS rule. However, for general L, we can prove such a result only for B of larger order than Λ^2.

Theorem 2. As $\Lambda^2/B \to 0$ for fixed η, L,

$$Z(\Lambda, B)/Z^*(\Lambda, B) \to 1 \tag{9.2}$$

Proof. First (4.4) states that $Z \leqslant Z^*$. For the reverse inequality, we change from state variables $\mathbf{z}$ to $\mathbf{d}$, where $d_l = z_{l+1} - z_l \geqslant 0$ for $l = 1,..., \Lambda - 1$, so that $d_1 + \cdots + d_{\Lambda-1} \leqslant B$. Then we can write

$$Z = \frac{B}{\Lambda} \sum_{\mathbf{d}} \sum_{\mathbf{N}} \eta^{2N} \int d\{x\}_{\mathbf{N}} \int d\{y\}_{\mathbf{N}} \prod_{l=1}^{\Lambda} J_{l,l+1} \tag{9.3}$$

where $J_{l,l+1} = 1$ if edges l and $l+1$ obey their mutual SOS rule, and $J_{l,l+1} = 0$ otherwise. Putting $K_{l,l+1} = 1 - J_{l,l+1}$ we have

$$\prod_l J_{l,l+1} = \prod_l (1 - K_{l,l+1}) \geqslant 1 - \sum_l K_{l,l+1} = 1 - \sum_l (1 - J_{l,l+1}) \tag{9.4}$$

so that

$$Z \geqslant Z^* - T \tag{9.5}$$

where $T \geqslant 0$ and

$$\begin{aligned} T &= B \sum_{\mathbf{d}} \sum_{\mathbf{N}} \eta^{2N} \int d\{x\}_{\mathbf{N}} \int d\{y\}_{\mathbf{N}} (1 - J_{1,2}) \\ &= B \sum_{\mathbf{d}} \left[I_0^{\Lambda} - I_0^{\Lambda-2} \sum_{k=-\infty}^{\infty} (I^2_{|k(B+2)|} - I^2_{|k(B+2)+d+1|}) \right] \qquad \text{[see (6.6)]} \\ &= B I_0^{\Lambda-2} \sum_{d=0}^{B} \binom{B+\Lambda-d-2}{\Lambda-2} \\ &\quad \times \left[\sum_{k=-\infty}^{\infty} I^2_{|k(B+2)+d+1|} - 2 \sum_{k=1}^{\infty} I^2_{|k(B+2)|} \right] \end{aligned} \tag{9.6}$$

The combinatorial factor is the number of combinations of end locations of the remaining $\Lambda - 2$ edges among the $B - d + 1$ sites not excluded by edges 1 and 2 at separation d. All the Bessel functions have argument 2 The square bracket in the last expression is

$$\begin{aligned} &I^2_{d+1} + I^2_{B-d+1} + \sum_{k=1}^{\infty} (I^2_{k(B+2)+d+1} - I^2_{k(B+2)}) \\ &\qquad + \sum_{k=1}^{\infty} (I^2_{k(B+2)+B-d+1} - I^2_{k(B+2)}) \\ &\qquad \leqslant I^2_{d+1} + I^2_{B-d+1} \end{aligned} \tag{9.7}$$

using the monotonicity of I_n in the index n. Then

$$\begin{aligned} T &\leqslant 2BI_0^{A-2} \cdot \binom{B+A-2}{A-2} \sum_{d=0}^{B} I_{d+1}^2 \\ &\leqslant Z^* \cdot \left[\frac{A(A-1)}{B+A-1} 2I_0^{-2} \sum_{d=0}^{B} I_{d+1}^2 \right] \\ &\leqslant Z^* o(1) \end{aligned} \tag{9.8}$$

as $A^2/B \to 0$. Thus from (9.5), $Z \geqslant Z^* \cdot \{1 - o(1)\}$, which proves the theorem. Note that the undesirable extra factor of A in T arises from (9.4); subsequent bounds preserve the order of magnitude of T. Thus an improved theorem would require an improved and manageable version of (9.4).

Using (5.8), we have the following corresponding high-density result.

Corollary 2.1. As $B^2/A \to 0$ for fixed η, L,

$$Z(A, B)/Z^\dagger(A, B) \to 1 \tag{9.9}$$

where

$$Z^\dagger(A, B) = V_0 I_0^B(2\eta L) \tag{9.10}$$

The approximation $Z \simeq Z^\dagger$ leads to $G(A, B) \simeq G(1, 1)$, which is consistent with (13.15).

10. THERMODYNAMIC LIMIT

Here we prove the existence of a thermodynamic limit of the negative free energy [see (5.2)]

$$\phi(\rho) = \lim \phi(A, B) \tag{10.1}$$

as A, $B \to \infty$, $A/B \to \rho$, where ρ is the mean density of edges or the slope of the surface. This enables us, ultimately, to expand $\bar{p}$ and G as power series in ρ (Section 13) and so demonstrate their slope dependence. First we write ω_l for an edge extending from $(0, z_l)$ to (L, z_l) on the surface, and put

$$\begin{aligned} A &= \{\boldsymbol{\omega} : 1 \leqslant z_1 \leqslant \cdots \leqslant z_A \leqslant B, \omega_1 \leqslant \omega_2 \leqslant \cdots \leqslant \omega_A\} \\ Q &= \{\boldsymbol{\omega} : \omega_A \leqslant \omega_1 + B\} \end{aligned} \tag{10.2}$$

where the inequalities on the ω_l's indicate the noncrossing (SOS) rule. Then the partition function is

$$Z = \mu(A \cap Q) \tag{10.3}$$

with μ defined by (7.4). We also define

$$Z^0 = \mu(A) \qquad \text{and} \qquad Z^R = \mu(A \cap R) \tag{10.4}$$

where

$$R = \{\boldsymbol{\omega} : 0 \leqslant \omega_1, \omega_\Lambda \leqslant B\} \tag{10.5}$$

Thus edges 1 and Λ are unconfined in Z^0, and are confined between barriers at 0 and B in Z^R. Since $0 \leqslant \omega_1$ and $\omega_\Lambda \leqslant B$ together imply $\omega_\Lambda - \omega_1 \leqslant B$, it follows that $R \subset Q$, whence

$$Z^R \leqslant Z \leqslant Z^0 \tag{10.6}$$

We denote the corresponding negative free energies by ϕ^R and ϕ^0.

First we prove a thermodynamic limit for ϕ^R by standard methods (cf. ref. 29, Chapter 3). We compare a $2B \times L$ surface having 2Λ edges with two adjoining $B \times L$ surfaces having Λ edges each. The set

$$T = \{\boldsymbol{\omega} : 1 \leqslant z_1 \leqslant \cdots \leqslant z_{2\Lambda} \leqslant 2B,\ 0 \leqslant \omega_1 \leqslant \cdots \leqslant \omega_{2\Lambda} \leqslant 2B\} \tag{10.7}$$

contains the set

$$\begin{aligned} U = \{\boldsymbol{\omega} : {} & 1 \leqslant z_1 \leqslant \cdots \leqslant z_\Lambda \leqslant B,\ 0 \leqslant \omega_1 \leqslant \cdots \leqslant \omega_\Lambda \leqslant B, \\ & B+1 \leqslant z_{\Lambda+1} \leqslant \cdots \leqslant z_{2\Lambda} \leqslant 2B,\ B \leqslant \omega_{\Lambda+1} \leqslant \cdots \leqslant \omega_{2\Lambda} \leqslant 2B\} \end{aligned} \tag{10.8}$$

Then $\mu(T) \geqslant \mu(U)$ and so

$$Z^R(2\Lambda, 2B) \geqslant [Z^R(\Lambda, B)]^2 \tag{10.9}$$

which implies $\phi^R_{k+1} \geqslant \phi^R_k$, where

$$\phi^R_k = B_k^{-1} \log Z^R(\Lambda_k, B_k) \tag{10.10}$$

and $\Lambda_k = 2^k \Lambda_0$ and $B_k = 2^k B_0$ for fixed Λ_0 and B_0. But, by (4.4), ϕ_k has the bound

$$\phi^R_k \leqslant \log(B_0/\Lambda_0 + 1) + \log I_0 + 1 \tag{10.11}$$

Thus ϕ^R_k has a finite limit as $k \to \infty$. For other sequences having the same limit see ref. 29, Chapter 3.

Next we relate the limiting ϕ^R to the limiting ϕ.

Lemma 1. For integer $\Delta > B(\log B)^{-1/2}$,

$$Z^0(\Lambda, B) \leqslant Z^R(\Lambda, B+2\Delta) + o(1) \tag{10.12}$$

as $\Lambda, B \to \infty$ and $\Lambda/B \to \rho$.

Proof. We write $Z^0 = \mu(W) + \mu(H)$, where

$$\begin{aligned} W &= \{\omega : 1 \leqslant z_1 \leqslant \cdots \leqslant z_\Lambda \leqslant B,\ -\Delta \leqslant \omega_1 \leqslant \cdots \leqslant \omega_\Lambda \leqslant B+\Delta\} \\ H &= \{\omega : 1 \leqslant z_1 \leqslant \cdots \leqslant z_\Lambda \leqslant B,\ \omega_1 \leqslant \cdots \leqslant \omega_\Lambda,\ \omega_l \text{ crosses} \\ &\quad -\Delta \text{ or } B+\Delta \text{ for at least one } l\} \end{aligned} \tag{10.13}$$

Now

$$W \subset \{\omega : -\Delta \leqslant z_1 \leqslant \cdots \leqslant z_\Lambda \leqslant B+\Delta,\ -\Delta \leqslant \omega_1 \leqslant \cdots \leqslant \omega_\Lambda \leqslant B+\Delta\} \tag{10.14}$$

whence

$$\mu(W) \leqslant Z^R(\Lambda, B+2\Delta) \tag{10.15}$$

For H, we first relax the SOS rule and put

$$\begin{aligned} J_l &= \{\omega : 1 \leqslant z_1 \leqslant \cdots \leqslant z_\Lambda \leqslant B,\ \omega_l \text{ crosses } -\Delta \text{ or } B+\Delta\} \\ K_\Delta &= \{\omega : \omega_l \text{ crosses } -\Delta \text{ or } B+\Delta\} \end{aligned} \tag{10.16}$$

Then we have

$$\mu(H) \leqslant \sum_l \mu^*(J_l) = \Lambda \mu^*(J_1) \tag{10.17}$$

because the right side multiply counts paths that leave $[-\Delta, B+\Delta]$. Thus

$$\mu(H) \leqslant \Lambda V_0 I_0^{\Lambda-1} \mu^*(K_\Delta) \tag{10.18}$$

and

$$\mu^*(K_\Delta) \leqslant \sum_{N=\Delta}^{\infty} \frac{(\eta L)^{2N}}{(N!)^2} \tag{10.19}$$

because any $\omega \in K_\Delta$ must contain at least Δ x-kinks and Δ y-kinks. Now

$$\mu^*(K_\Delta) \leqslant e^{2\eta L}/\Delta! \tag{10.20}$$

which gives a bound of the form

$$\mu(H) \leqslant c^B/\Delta! \tag{10.21}$$

for constant c and for large enough B, with $\Lambda/B \to \rho$. Then $\mu(H) \to 0$ as $B \to \infty$ for Δ as specified, which proves Lemma 1.

Combined with (10.6), Lemma 1 gives

$$\frac{1}{B}\log Z^R(\Lambda, B) \leqslant \frac{1}{B}\log Z(\Lambda, B) \leqslant \frac{1}{B}\log Z^R(\Lambda, B+2\Delta) + o(1) \tag{10.22}$$

If $\Delta \sim B(\log B)^{-1/2}$, then $(B+2)/B \to 1$ and $\Lambda/(B+2\Delta) \to \rho$. Thus $\phi(\rho)$ exists and equals $\phi^R(\rho)$. Using (10.6) again implies that $\phi^0(\rho)$ exists and

$$\phi^0(\rho) = \phi(\rho) = \phi^R(\rho) \tag{10.23}$$

Concavity of $\phi(\rho)$ follows by the usual arguments (ref. 29, Chapter 3).

To prove that $\bar{p}(\Lambda, B)$ and $\bar{\zeta}(\Lambda, B)$ have unique thermodynamic limits requires a "continuity of pressure" argument (cf. ref. 29, p. 58, and ref. 11), which is lacking here. Assuming, as seems likely, that such limits exist, one can relate them to ϕ as follows. Put $F(\Lambda, B) = \log Z(\Lambda, B)$,

$$f(v) = \lim F(\Lambda, B)/\Lambda = v\phi(1/v) \tag{10.24}$$

and

$$\tilde{p}(v) = \lim \bar{p}(\Lambda, B) \tag{10.25}$$

under the limit $\Lambda \to \infty$, $B/\Lambda \to v$. Suppose that $\tilde{p}(\cdot)$ is continuous and the convergence in (10.25) is uniform for $v \in [a, b]$ in the sense that

$$\sup_{a\Lambda \leqslant j \leqslant b\Lambda} |F(\Lambda, j+1) - F(\Lambda, j) - \tilde{p}(j/\Lambda)| \to 0 \qquad \text{as} \quad \Lambda \to \infty \tag{10.26}$$

Writing $[\Lambda v]$ for the integer part of Λv, we have

$$\begin{aligned} f(v) - f(a) &= \lim_{\Lambda \to \infty} \frac{1}{\Lambda}\{F(\Lambda, [\Lambda v]) - F(\Lambda, [\Lambda a])\} \\ &= \lim_{\Lambda \to \infty} \left\{ \frac{1}{\Lambda} \sum_{j=[\Lambda a]}^{[\Lambda v]-1} \tilde{p}\left(\frac{j}{\Lambda}\right) \right. \\ &\quad \left. + \frac{1}{\Lambda} \sum_{j=[\Lambda a]}^{[\Lambda v]-1} \left[F(\Lambda, j+1) - F(\Lambda, j) - \tilde{p}\left(\frac{j}{\Lambda}\right) \right] \right\} \\ &= \int_a^v \tilde{p}(u)\, du \end{aligned} \tag{10.27}$$

for $v \in [a, b]$ by (10.26). Hence $f'(v)$ exists in $[a, b]$ and

$$\tilde{p}(v) = f'(v) \tag{10.28}$$

(This argument is essentially an example of convergence of a sequence implying Cesaro convergence). Similarly, if the limit

$$\bar{\zeta}(\rho) = \lim_{A/B \to \rho} \bar{\zeta}(A, B) \tag{10.29}$$

exists and the convergence is uniform, then

$$\log \bar{\zeta}(\rho) = -\phi'(\rho) \tag{10.30}$$

The results (10.28) and (10.30) are relevant to the equivalence of ensembles (Section 12). We put $\bar{p}(\rho) = \tilde{p}(1/\rho)$.

The $A \leftrightarrow B$ symmetry links quantities at small and large ρ. Thus (5.7)–(5.10) imply

$$\begin{aligned} G(\rho) &= \rho G(1/\rho) \\ \phi(\rho) &= \phi(1/\rho)/\rho \\ \bar{p}(\rho) &= -\log \bar{\zeta}(1/\rho) \end{aligned} \tag{10.31}$$

11. CONCIDENCE PROBABILITIES AND FORMULAS FOR Z^0

Since $\phi(\rho) = \phi^0(\rho)$, analysis of the model may be based upon Z^0.

Lemma 2. We have

$$Z^0 = \sum_{\mathbf{z}} \det A(\mathbf{z}) \tag{11.1}$$

where the $\mathbf{z}$ sum extends over (2.2) and $A(\mathbf{z})$ is a $A \times A$ matrix with components

$$A_{lm}(\mathbf{z}) = I_{|z_l - z_m| + |l-m|}(2\eta L) \tag{11.2}$$

To show this, consider a symmetric randomized random walk, such as that described in ref. 5, Chapter 2, Section 7(b), in which a simple symmetric random walk has steps at the points of a Poisson process of rate 2η running for time L. This is clearly a Markov process. If we have A independent such processes, starting at $z_1, \ldots, z_A$, it is not hard to see that the joint probability distribution of their paths and the event that they are again at $z_1, \ldots, z_A$, respectively, after L is the same, apart from a factor of

$\exp(-2\eta L\Lambda)$, as the joint probability of Λ independent edges in our model without the SOS constraint.

Now apply to the above random walk a result of Karlin and McGregor,[24] which gives the probability that a number of independent Markov processes reach a given set of positions without their paths coinciding. The SOS constraint in Z^0 is equivalent to no path coincidences if we start all paths one NS step further away from each other. Because of the equivalence of the probability distributions up to a factor, the Karlin–McGregor result gives the summands in Z^0 once the factor is removed. Lemma 2 now follows from the fact[5] that the transition probabilities of the Markov process are

$$p_{zz'}(L) = e^{-2\eta L} I_{|z-z'|}(2\eta L) \tag{11.3}$$

We remark that, although Z^0 is not the normalizing constant of any growth process of which we are aware, its calculation *is* related to a process, but one with a quite different interpretation.

For the cluster expansion, to be developed in Section 13, we need Z^0 up to $\Lambda = 3$. First we have

$$\begin{aligned} Z^0(2, B) &= \sum_{z_2=1}^{B} \sum_{z_1=1}^{z_2} (I_0^2 - I_{z_2-z_1+1}^2) \\ &= \tfrac{1}{2}B(B+1)\, I_0^2 - (B+1)\, S_0 + S_1 \end{aligned} \tag{11.4}$$

where

$$S_n = \sum_{j=1}^{B} j^n I_j^2 \tag{11.5}$$

Next we have

$$Z^0(3, B) = \tfrac{1}{3}B(B+1)(B+2)\, I_0^3 - (R_1 + R_2 + R_3) I_0 + 2R_4 \tag{11.6}$$

where

$$\begin{aligned} R_1 &= \sum_{\mathbf{z}} I_{z_2-z_1+1}^2 \\ R_2 &= \sum_{\mathbf{z}} I_{z_3-z_2+1}^2 \\ R_3 &= \sum_{\mathbf{z}} I_{z_3-z_1+1}^3 \\ R_4 &= \sum_{\mathbf{z}} I_{z_2-z_1+1} I_{z_3-z_2+1} I_{z_3-z_1+1} \end{aligned} \tag{11.7}$$

and all the Bessel functions have argument $2\eta L$ and the sums are over $1 \leqslant z_1 \leqslant z_2 \leqslant z_3 \leqslant B$. Rearranging the summations and changing summation variables gives

$$R_1 = \sum_{z_3=1}^{B} \sum_{j=1}^{z_3} (z_3 - j + 1) I_j^2$$
$$= \tfrac{1}{2}(B+1)(B+2)S_0 - \tfrac{1}{2}(2B+3)S_1 + \tfrac{1}{2}S_2 \tag{11.8}$$

Reversing the order of the z_i's shows that $R_2 = R_1$. In a similar fashion we have

$$R_3 = -(B+2)S_0 + (B+3)S_1 - S_2 \tag{11.9}$$

and

$$R_4 = B\Sigma_1 - 2\Sigma_2 \tag{11.10}$$

where

$$\Sigma_1 = \sum_{k=1}^{B} \sum_{j=1}^{B-k+1} I_j I_k I_{j+k}$$
$$\Sigma_2 = \sum_{k=1}^{B} \sum_{j=1}^{B-k+1} j I_j I_k I_{j+k} \tag{11.11}$$

Combining the above gives

$$Z^0(3, B) = \tfrac{1}{3}B(B+2)(B+3)\, I_0^2 - B(B+2)\, I_0 S_0 + BS_1 + 2B\Sigma_1 - 4\Sigma_2 \tag{11.12}$$

12. THE GRAND ENSEMBLE

The *grand partition function*

$$\Xi(\zeta, B) = 1 + \sum_{A=1}^{\infty} \zeta^A Z(A, B) \tag{12.1}$$

is the normalizing constant of the invariant distribution of a reducible process comprising an ensemble of the original Markov processes with different A, having weights ζ^A. For $\zeta < 1/I_0(2\eta L)$, the convergence of the series for Ξ follows from (4.4), giving the bound

$$\Xi(\zeta, B) \leqslant \{1 - \zeta I_0(2\eta L)\}^{-B} \tag{12.2}$$

Theorem 3. For $\zeta < 1/I_0(2\eta L)$, the limit

$$p(\zeta) = \lim_{B \to \infty} \frac{1}{B} \log \Xi(\zeta, B) \tag{12.3}$$

exists and

$$p(\zeta) = \sup_{\rho} \{\rho \log \zeta + \phi(\rho)\} \tag{12.4}$$

For our purposes, the main value of this result is that it leads to cluster expansions (Section 13). The proof follows Theorem 3.4.6 of ref. 29, using the concavity of $\phi(\cdot)$ and the bound (4.4). Defining $p^R(\zeta)$ and $p^0(\zeta)$ in terms of Z^R and Z^0 in like manner, we have

$$p(\zeta) = p^R(\zeta) = p^0(\zeta) \tag{12.5}$$

Proof of uniqueness of the maximal $\rho(\zeta)$ in (12.4) would require differentiability (absence of phase transition) of $p(\zeta)$. Assuming, as seems likely, that this holds, we have

$$\begin{aligned} p(\zeta) &= \rho(\zeta) \log \zeta + \phi\{\rho(\zeta)\} \\ \log \zeta &= -\phi'\{\rho(\zeta)\} \\ \rho(\zeta) &= \zeta p'(\zeta) \end{aligned} \tag{12.6}$$

Then using (10.28) and (10.30) gives

$$\begin{aligned} p(\zeta) &= \bar{p}\{\rho(\zeta)\} \\ \log \zeta &= \log \bar{\zeta}\{\rho(\zeta)\} \end{aligned} \tag{12.7}$$

i.e., the ensembles are "equivalent". Thus ζ and $p(\zeta)$ have the statistical interpretations given in Section 5. In a similar fashion

$$G\{\rho(\zeta)\} = \frac{g\eta}{L} \frac{\partial}{\partial \eta} p(\zeta) \tag{12.8}$$

where

$$G(\rho) = \lim_{A/B \to \rho} G(A, B) \tag{12.9}$$

is the growth rate in the thermodynamic limit.

A sharper version of (12.5) can be obtained via a direct proof of the existence of $p(\zeta)$ as follows (though this does not establish the equivalence of ensembles). In place of Lemma 1, one finds, by a more detailed counting of edges that escape from $[-\Delta, B+\Delta]$,

$$Z^0(\Delta, B) \leqslant \sum_{k=0}^{\infty} \binom{B+k-1}{k} (k+1)[\mu(K_\Delta)]^k Z^R(\Delta-k, B+2\Delta) \quad (12.10)$$

Multiplying through by ζ^Δ and summing gives

$$\Xi^R(\zeta, B) \leqslant \Xi^0(\zeta, B) \leqslant \Xi^R(\zeta, B+2\Delta)[1+\gamma(B, \Delta)] \quad (12.11)$$

where

$$\gamma(B, \Delta) = 2\zeta B\mu(K_\Delta)[1-\zeta\mu(K_\Delta)]^{-B} \quad (12.12)$$

Then $\gamma \to 0$ as $B \to \infty$ and $\Delta!/B \to \infty$, a much weaker condition than in Lemma 1. Thus Ξ, Ξ^R, and Ξ^0 are very close for larger B, and growth rates can be obtained via Ξ^0 and (11.1).

13. CLUSTER EXPANSIONS

A formal series or cluster expansion for $p(\zeta)$ takes the usual form and leads to a series for $G(\rho)$. This provides successive corrections to the growth rate of small-angle surfaces. Since we have an explicit expression for Z^0, we use (12.1) and (12.3) to get

$$p(\zeta) = p^0(\zeta) = b_1\zeta + b_2\zeta^2 + b_3\zeta^3 + \cdots \quad (13.1)$$

where

$$\begin{aligned} b_1 &= Z^0(1, B)/B = I_0(2\eta L) \\ b_2 &= \lim_{B\to\infty} \frac{1}{B}\left[Z^0(2, B) - \frac{1}{2} Z^0(1, B)^2 \right] \\ b_3 &= \lim_{B\to\infty} \frac{1}{B}\left[Z^0(3, B) - Z^0(2, B)\, Z^0(1, B) + \frac{1}{3} Z^0(1, B)^3 \right] \end{aligned} \quad (13.2)$$

and so on. Continuing formally gives

$$p(\zeta) = b_1\zeta + 2b_2\zeta^2 + 3b_3\zeta^3 + \cdots \quad (13.3)$$

whence, with (12.7),

$$\bar{p}(\rho) = \rho - (b_2/b_1^2)\,\rho^2 + (4b_2^2/b_1^4 - 2b_3/b_1^3)\,\rho^3 + \cdots \quad (13.4)$$

Differentiating (13.1) with respect to η and denoting η derivatives by a prime, we have

$$G(\rho) = (g\eta/L)(b_1'\zeta + b_2'\zeta^2 + b_3'\zeta^3 + \cdots) = (g\eta/L)(c_1\rho + c_2\rho^2 + c_3\rho^3 + \cdots) \tag{13.5}$$

where

$$\begin{aligned} c_1 &= b_1'/b_1 = 2LI_1(2\eta L)/I_0(2\eta L) \\ c_2 &= (b_2/b_1^2)' \\ c_3 &= (b_3/b_1^3)' - 2(b_2^2/b_1^4)' \end{aligned} \tag{13.6}$$

Now we evaluate c_2 and c_3. From (11.4) and Neumann's identity (6.8) we have

$$b_2 = I_0^2(2\eta L) - \tfrac{1}{2}I_0(4\eta L) \tag{13.7}$$

and hence

$$c_2 = -2LI_0^{-3}(2\eta L)[I_0(2\eta L)\, I_1(4\eta L) - I_0(4\eta L)\, I_1(2\eta L)] \tag{13.8}$$

From (11.4), (11.12), and (6.8) we have

$$b_3 = \tfrac{5}{6}I_0^3(2\eta L) - \tfrac{1}{2}I_0(2\eta L)\, I_0(4\eta L) + 2\Sigma(2\eta L) \tag{13.9}$$

where

$$\Sigma(x) = \sum_{j=1}^{\infty} \sum_{k=1}^{\infty} I_j(x)\, I_k(x)\, I_{j+k}(x) \tag{13.10}$$

which converges rapidly. Then an explicit expression for c_3 follows from the identity

$$\frac{d}{dx} I_n(x) = \frac{1}{2}[I_{n+1}(x) + I_{n-1}(x)] \tag{13.11}$$

For example, if $2\eta L = 10$, then $c_1/(2L) = 0.948600$, $c_2/(2L) = -0.143234$, and $c_3/(2L) = -0.219464$. Thus, for small ρ,

$$G(\rho) = (2ig)^{1/2}(0.9486\rho - 0.1432\rho^2 - 0.2195\rho^3 + \cdots) \tag{13.12}$$

This is plotted in Fig. 8, and shows good agreement with the simulations, surprisingly up to about $\rho = 0.8$.

We recall that the first terms in (13.4) and (13.5) were obtained rigorously for the case of two edges [see (6.15)]. For small ηL we have $c_1 \sim 2\eta L^2$, $c_2 \sim -2\eta L^2$, and $c_3 \sim 2\eta L^2$, which gives

$$G \sim iL(\rho - \rho^2 + \rho^3 + \cdots) \tag{13.13}$$

for small ρ. This is consistent with (7.1). Equation (13.5) suggests that

$$G(\rho)/\rho \to G(1, 1) \qquad \text{as} \quad \rho \to 0 \tag{13.14}$$

which is a stronger version of the independent-edges result, Theorem 2. However, proving this would require a theory of the series expansion.

Using (10.31), we deduce from (13.5) that

$$G(\rho) = (g\eta/L)(c_1 + c_2\rho^{-1} + c_3\rho^{-2} + \cdots) \tag{13.15}$$

for large ρ. In particular, for $2\eta L = 10$,

$$G(\rho) = (2ig)^{1/2}(0.9486 - 0.1432\rho^{-1} - 0.2195\rho^{-2} + \cdots) \tag{13.16}$$

This is compared with the simulations in Fig. 8. The agreement is good for $\rho > 1.2$ as expected. Of course, the absolute error in (13.16), being of third degree, is greater than that in (13.12), being of fourth degree.

The radius of convergence $\mathscr{R}$ of the power series for $G(\rho)$ cannot exceed 1. For, if it did, the Laurent series for $G(\rho) - \rho G(1/\rho) = 0$ would be analytic in the annulus $1/\mathscr{R} < |\rho| < \mathscr{R}$ of the complex plane. Since $G(\rho) \neq C \cdot (1 + \rho)$, it would then follow that $G(\rho) = 0$ for all ρ, a contradiction.

For small ηL, (7.1) gives $G(\rho) \sim Li/(1 + \rho)$, with $\mathscr{R} = 1$. The main unsolved problem is to find a lower bound on $\mathscr{R}$ in general.

Because of the $A \leftrightarrow B$ symmetry, the above developments and those of Section 12 can, just as readily, be based upon the *isobaric partition function*

$$\Gamma(\Lambda, p) = 1 + \sum_{B=1}^{\infty} e^{-Bp} Z(\Lambda, B) \tag{13.17}$$

instead of $\Xi(\zeta, B)$. This exists for $p > \log I_0(2\eta L)$ because $Z \leqslant Z^{\dagger}$. If we call $-(\log \Gamma)/\Lambda$ the *Gibbs free energy*, then the usual thermodynamic relations hold in the limit $\Lambda \to \infty$. In view of (11.1), $\Gamma^0(\Lambda, p)$, based upon Z^0, can be represented by an unconstrained sum of determinants.

14. SIMULATIONS

Because of the Markov property, creations occur uniformly on $\bigcup_l S_l$ and at time intervals having exponential distribution with instantaneous rate $q = i \sum_l D_l$. Rather than computing the S_l's, one can generate locations uniformly on all the edges and at exponential times with mean $1/(i\Lambda L)$, and then reject creations that violate the SOS rule, so-called rejection sampling.

Ergodic theory for Markov chains implies that

$$\langle N \rangle = \lim_{k \to \infty} \frac{1}{t_k} \sum_{i=1}^{k} (t_i - t_{i-1}) N(t_i) \tag{14.1}$$

where the t_i are the times at which kinks are lost or gained and the process $N(t)$ is the total number of x-kinks at time $t+0$. Then (5.1) gives G. Also the mean creation rate is

$$i \left\langle \sum_l D_l \right\rangle = \lim_{t \to \infty} M(t)/t \tag{14.2}$$

where the process $M(t)$ is the total number of creations up to time t. Then (5.3) gives R.

In the simulations we took $i = L = 1$, without loss of generality, and $g = 0.02$, which implies $2\eta L = 10$. This places us near regime II. We also took $\Lambda = 10$ and B values 1–12 and 14, 16, 20, 25, 33, 50, and 100, leading to values of ρ in the range 0.1–10. For each value of B we simulated 10^5 transitions and used (14.1) and (14.2) to compute growth rates and creation rates.

Figure 8 shows $G/(2ig)^{1/2}$ plotted against ρ and Fig. 9 shows R plotted against ρ. Both graphs are in accord with the general observations in previous sections, and demonstrate the pronounced effects of interaction between edges as density of edges increases, i.e., as the slope of the surface increases.

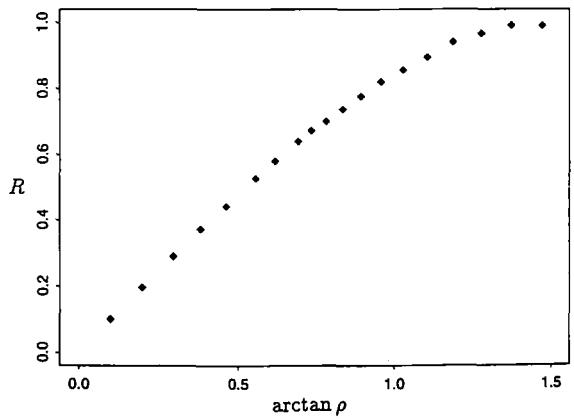

Fig. 9. The dimensionless creation rate versus angle of the surface in the model with $i = L = 1$, $g = 0.02$, and $\Lambda = 10$, generated by simulations.

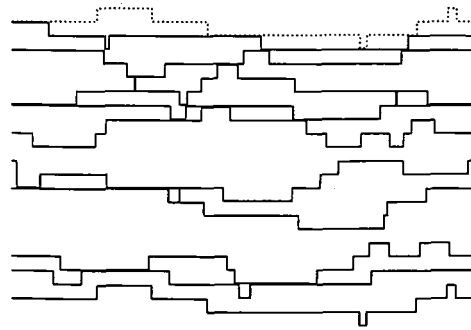

Fig. 10. Example of a state generated by simulations with $i = L = 1$, $g = 0.02$, $\Lambda = 10$, and $B = 20$.

Figure 10 shows a state of the process with $B = 20$ and $\Lambda = 10$ after 10^5 transitions. The broken line is the periodic image of edge Λ. For smaller g we would see many more kinks, greater excursions by edges, and more frequent instances (though smaller intervals) of interactions between edges.

15. DIAGONALLY SLOPING SURFACES

Suppose that every edge has an excess of K x-kinks over y-kinks. Then the surface has a slope in the EW direction or, regarding $\Lambda \times L$ as the base, a slope of K steps in the EW direction. The appropriate modifications of the Markov process are fairly obvious.[16] The EW periodic boundary conditions have a K-step shift, so that edges join continuously to their periodic extensions. Here we outline the main results.

The stationary distribution (4.1) applies on the modified state space. The two-edge case (Section 6) now involves the more general version of (6.4) from ref. 4, Chapter 3.

Small ηL (Section 7) is replaced by $\eta = 0$ or $i = 0$. Then, after time L/g, all y-kinks are removed from any initial state and the subsequent process comprises the deterministic motion of the $K\Lambda$ x-kinks alone. Thus $G = \alpha g$, where $\alpha = K\Lambda/LB$ is the number of kinks per unit area. This constrasts sharply with the $K = 0$ result (7.2) and is another instance of permanent steps dominating growth.[16]

For high edge density, (5.11) becomes (cf. ref. 16, Theorem 5)

$$G(\Lambda, 1) = (2ig)^{1/2} I'_K / I_K \tag{15.1}$$

For low edge density, (9.2) holds with

$$Z^* = V_0 I_K^A \tag{15.2}$$

The results for the thermodynamic limit (Section 10) are unchanged, except that (10.31) does not apply. The base or substrate implied by Z^0 or Z^R is now a parallellogram.

In Lemma 2, the matrix is replaced by

$$A_{lm} = I_{K+z_l-z_m+l-m}(2\eta L) \tag{15.3}$$

which leads to the cluster coefficients

$$\begin{aligned} b_1 &= I_K(2\eta L) \\ b_2 &= I_K^2(2\eta L) - \tfrac{1}{2} I_{2K}(4\eta L) \\ c_1 &= 2LI'_K(2\eta L)/I_K(2\eta L) \\ c_2 &= -2LI_K^{-2}(2\eta L)[I_K(2\eta L)\, I'_{2K}(4\eta L) - I'_K(2\eta L)\, I_{2K}(4\eta L)] \end{aligned} \tag{15.4}$$

ACKNOWLEDGMENTS

We thank S. Fletcher for information and discussions on size dependence and growth rate dispersion. We also thank a referee for bringing the free fermion method to our notice and for clarifying the method.

REFERENCES

1. C. H. Bennett, M. Bütticker, R. Landauer, and H. Thomas, *J. Stat. Phys.* **24**:419 (1981).
2. H. van Beijeren and I. Nolden, In *Structure and Dynamics of Surfaces II*, W. Schommers and P. von Blanckenhagen, eds. (Springer, Berlin, 1987), Chapter 7, p. 259.
3. E. T. Copson, *An Introduction to the Theory of Functions of a Complex Variable* (Clarendon, Oxford, 1962).
4. W. Feller, *An Introduction to Probability Theory and its Applications*, Vol. 1 (Wiley, New York, 1958).
5. W. Feller, *An Introduction to Probability Theory and its Applications*, Vol. 2 (Wiley, New York, 1958).
6. F. C. Frank, *Disc. Faraday Soc.* **5**:48 (1949).
7. F. C. Frank, *J. Crystal Growth* **22**:233 (1974).
8. C. Garrod, *J. Stat. Phys.* **63**:987 (1991).
9. J. Garside, In *Crystal Growth and Materials*, E. Kaldis and H. J. Scheel, eds. (North-Holland, Amsterdam, 1977), p. 484.
10. D. J. Gates, *J. Stat. Phys.* **52**:245 (1988).
11. D. J. Gates and O. Penrose, *Commun. Math. Phys.* **16**:231 (1970).
12. D. J. Gates and M. Westcott, *Proc. R. Soc. London. A* **416**:443 (1988).
13. D. J. Gates and M. Westcott, *Proc. R. Soc. Lond. A* **416**:463 (1988).

14. D. J. Gates and M. Westcott, *J. Stat. Phys.* **59**:73 (1990).
15. D. J. Gates and M. Westcott, Markov models of steady crystal growth, *Ann. Appl. Prob.* **3**:339 (1993).
16. D. J. Gates and M. Westcott, *J. Stat. Phys.* **77**:199 (1994).
17. P. G. de Gennes, *J. Chem. Phys.* **48**:2257 (1968).
18. G. H. Gilmer, *J. Crystal Growth* **49**:465–474 (1980).
19. G. H. Gilmer and K. A. Jackson, *Crystal Growth and Materials*, E. Kaldis and H. J. Scheel, eds. (North-Holland, Amsterdam, 1976), p. 80.
20. N. Goldenfeld, *J. Phys. A* **17**:2807 (1984).
21. J. D. Hoffman, G. T. Davis, and J. I. Lauritzen, Jr., In *Treatise on Solid-State Chemistry*, Vol. 3. *Crystalline and Non-crystalline Solids*, N. B. Hanay, ed. (Plenum Press, New York, 1976), p. 335.
22. J. D. Hoffman, *Polymer* **24**:3 (1983).
23. B. Joos, T. L. Einstein, and N. C. Bartelt, *Phys. Rev. B* **43**(10):8153 (1991).
24. S. Karlin and J. McGregor, *Pac. J. Math.* **19**:1141 (1959).
25. F. Khoury and E. Passaglia, Ref. 21, p. 497.
26. M. Kotrla and M. Levi, *J. Stat. Phys.* **64**:579 (1991).
27. J. I. Lauritzen, Jr., *J. Appl. Phys.* **44**:4353 (1973).
28. A. P. Prudnikov, Yu. A. Brychkov, and O. I. Marichev, *Integrals and Series*, Vol. 1: *Elementary Functions* (Gordon and Breach, New York, 1986).
29. D. Ruelle, *Statistical Mechanics* (Benjamin, New York, 1969).
30. D. M. Sadler, *Polymer* **28**:1440 (1987).
31. J. Villain and P. Bak, *J. Phys.* (Paris) **42**:657 (1981).
32. J. D. Weeks and G. H. Gilmer, *Adv. Chem. Phys.* **40**:157 (1979).
33. P. Whittle, Reversibility in Markov processes, Unpublished manuscript (1955).
34. P. Whittle, *Systems in Stochastic Equilibrium* (Wiley, Chichester, 1986).